Hindawi
Adsorption Science & Technology
Volume 2023, Article ID 8468644, 8 pages
https://doi.org/10.1155/2023/8468644

Research Article

Inorganic Adsorption on Thermal Response and Wear Properties of Nanosilicon Nitride-Developed AA6061 Alloy Nanocomposite

F. Mary Anjalin,[1] A. Mohana Krishnan,[2] G. Arunkumar,[3] K. Raju,[4] M. Vivekanandan,[5] S. Somasundaram,[6] T. Thirugnanasambandham,[7] and Elangomathavan Ramaraj[8]

[1]*Department of Physics, Saveetha School of Engineering, SIMATS, Chennai, 602105 Tamilnadu, India*
[2]*Department of Mechanical Engineering, K.Ramakrishnan College of Engineering, Trichy, 621112 Tamilnadu, India*
[3]*Department of Mechanical Engineering, K.Ramakrishnan College of Technology, Trichy, 621112 Tamilnadu, India*
[4]*Department of Mechanical Engineering, M.Kumarasamy College of Engineering, Karur, 639113 Tamilnadu, India*
[5]*Department of Mechanical Engineering, Kongunadu College of Engineering and Technology, Trichy, 621215 Tamilnadu, India*
[6]*Department of Mechanical Engineering, Sri Venkateswara Institute of science and technology, Thiruvallur, 631203 Tamil Nadu, India*
[7]*Department of Mechanical Engineering, Ponnaiyah Ramajayam Institute of Science and Technology, Thanjavur, 613203 Tamil Nadu, India*
[8]*Department of Biology, College of Natural and Computational sciences, Debre Tabor University, Amhara region, Ethiopia*

Correspondence should be addressed to Elangomathavan Ramaraj; elanmath@dtu.edu.et

Received 2 September 2022; Revised 15 October 2022; Accepted 24 November 2022; Published 25 January 2023

Academic Editor: Debabrata Barik

Inorganic-based ceramic reinforcements are promising superior thermal behaviour and are lightweight and developed with aluminium alloy matrix for automobile applications. The AA6061 alloy nanocomposite containing 0 wt%, 4 wt%, 8 wt%, and 12 wt% of silicon nitride nanoparticles(50 nm) was synthesized by stir cast. The influences of thermal adsorption on silicon nitride (nano) additions, density, thermal response, hardness, and wear characteristics of AA6061 matrix nanocomposites are studied. Based on the rule of mixture, the density of nanocomposites is evaluated. The differential thermal and thermogravimetric analysis techniques are used to find the thermal response nanocomposite. The differential scanning calorimeter is used to find the heat flow between 400°C and 700°C. The micro Vickers hardness and wear characteristics of AA6061 nanocomposite were experimentally investigated by ASTM E384 and ASTM G99-05 standards. The adsorption of inorganic nanosilicon nitride particles (12 wt%) in AA6061 alloy showed a decreased mass loss with increased temperatures 0° to 700°C. The differential thermal analysis of nanocomposite reveals the transformation of solid-to-liquid phase under high temperature (528°C).

1. Introduction

A matrix material is becoming essential in Metal Matrix Composites (MMCs) bonded with different reinforcements like organic and inorganic to obtain specific thermal, mechanical, and tribological characteristics. According to the past fifty years survey by Pradeep et al. [1], the demand for MMC's cast increased from 0 to 10 mega kilograms yearly. Commonly, the MMCs are divided into three categories like Aluminium Matrix Composite (AMC), Titanium Matrix Composite (TMC), and Magnesium Matrix Composite (MMC). Mainly, various researchers designated and investigated aluminium and its alloy-based matrix materials due to its exhibited mechanical, electrical, thermal, and corrosion resistance properties, which have been prominent substitutions of conventional matrix materials as listed above. However, it has reduced wear and thermal stability in the applications of high-temperature circumstances.

Based on previous literature reported by Sharma [2] and Shalaby et al. [3], the aluminium alloy materials were retained by aerospace and automotive (engine piston) applications and the materials undergone high thermal stress. While improving the thermal stability and withstanding high thermal stress, it could be added with secondary reinforcement phases like borides (SiB_3 and TiB_2), carbides (SiC and TiC), nitrides (Si_3N_4 and BN), and oxides (Al_2O_3 and TiO_2) grant to higher isotropic characteristics [4–8]. Based on the above literature review, it was identified by nitride-based ceramic-reinforced developed AMC has good thermal stability and is suitable for high-temperature applications. Ramesh et al. [9, 10] studied the physical and mechanical performance of sintered AA6061/Si_3N_4 composite. They reported that the increased weight percentages of Si_3N_4 (10 wt%) in AA6061 alloy showed an excellent tensile strength of 217 Mpa. Bai et al. [11] developed AMC with Al_2O_3/25wt% Si_3N_4 composite and found more pores on grain boundary and increased density due to increased wt% of (25 wt%) Si_3N_4. Fayomi et al. [12] fabricated and studied the microstructural, mechanical, and electrical properties of ZrB_2/Si_3N_4-reinforced aluminium alloy (AA8011) hybrid composite via the double-step stir cast technique. The optical microscope showed uniform distribution of multireinforcement in the AA8081 matrix. It has helped to improve the performance of the composite.

Similarly, the double-step stir cast technique increases wettability, and particle distribution may vary due to the selection of input process parameters. Among the various combinations, silicon nitride owing excellent thermal stability under elevated temperatures (27°C) reported by Zhu et al. [13]. Silicon nitride-bonded aluminium alloy composites were prominently used in high friction and temperature applications like bearings, turbine blades, and heat exchangers [14]. The abovementioned processing techniques and their effect on reinforcement in aluminium alloy matrix properties were explained in detail. It was found that the AMCs are developed by liquid state stir cast technique to facilitate lightweight with complex shape components on low processing cost. Han et al. [15] found that the Si_3N_4 reinforced with an aluminium alloy matrix resulted in good thermal shock resistance, superior thermal conductivity, and excellent wear resistance properties. It has been noted from various kinds of literature that there have few reports available on AMCs with Si_3N_4 nanocomposite manufacturing by liquid state stir cast. The present research is to develop AA6061/Si_3N_4 nanocomposite with improved density, hardness, wear resistance, and thermal adsorption properties.

2. Experimental Details

2.1. Choice of Matrix and Reinforcements. Aluminium alloy (AA6061) was chosen as the matrix material. It contains 1% magnesium and 0.6% silicon as major constitution having low density (2.70 g/cc), high strength, good thermal conductivity (160 W/m.K), and excellent corrosion resistance [16]. The chemical constitutions of AA6061 alloy are mentioned in Table 1.

The inorganic 50 nm silicon nitride (Si_3N_4) particles were chosen as reinforcement to obtain a better thermal response and wear properties [15]. The physical, mechanical and thermal characteristics of AA6061 and Si_3N_4 are shown in Table 2.

2.2. Processing Techniques of AA6061 Alloy Nanocomposite. Figures 1(a) and 1(b)illustrate the fabrication setup and flow processing chart for AA6061 alloy nanocomposite fabrication. Initially, the prepared AA6061 alloys are placed in a vortex crucible connected to an electrical furnace. The placed aluminium alloy was preheated to a red hardness temperature of 350°C for 20 mins and then the electrical furnace temperature was hiked to 750°C. It results in the AA6061 alloys melting at the liquid stage. After the temperature of the furnace was reduced to 550°C at 30 mins like semisolid condition and the molten metal was stirred with a graphite twin blade at 600 rpm revealed that the moisture content of the metal was removed. It may lead to a decrease in the porosity of the composite. The externally muffle furnace-preheated (300°C) Si_3N_4 nanoparticles are fed manually via feeder arrangement into a crucible chamber and mixed with molten AA6061 alloy via continuous mechanical stirrer action with an applied stir speed of 600 rpm at 30 mins. It resulted in increased uniform particle distribution and decreased voids [17]. Finally, the mixed molten AA6061 alloy and silicon nitrides were supplied to the casting die at 600°C. The developed composites are cooled by natural convection. The weight percentages of AA6061/Si_3N_4 nanocomposites are mentioned in Table 3. The developed AA6061 nanocomposite is sized as per test standards. A detailed phase transformation diagram for aluminium alloy (AA6061) nanocomposites is presented in Figure 2.

2.3. Discussions of Test Results. The advanced cast aluminium alloy (AA6061) and silicon nitride nanoparticle-reinforced ASTM test standards evaluated AA6061 alloy nanocomposites and their values were mentioned in Table 4. It was found that the density, micro Vickers hardness, and thermal performance of composites were increased. The porosity and wear rate were decreased with improved content of silicon nitride particles.

2.4. Effect of Si_3N_4 on Density and Porosity of AA6061 Alloy Nanocomposites. Figure 3 represents the density and porosity level for liquid state stir cast-developed AA6061 alloy and its AA6061/Si_3N_4 nanocomposite. It was noted from Figure 3 that the density of composites was increased and the porosity of the composite was decreased by the additions of Si_3N_4 on the AA6061 alloy matrix. So the density of the composite was inversely proportional to the porosity of the composite. The density of cast AA6061 alloy was 2.67 g/cc and 4 wt% Si_3N_4 showed 2.785 g/cc. While the inclusions of reinforcement may increase the density of the composite, meantime, the porosity of the composite was reduced from 1.15% to 1.03%.

Further inclusions of (8 wt% and 12 wt%) silicon nitrides into aluminium alloy (AA6061) matrix resulted in improvement in (2.804 g/cc and 2.832 g/cc) density of nanocomposite and obeyed the rule of mixture. The porosity of AA6061 alloy and its Si_3N_4-reinforced nanocomposites is measured by the

Table 1: Chemical constitutions of AA6061 alloy.

Constitutions	Al	Mg	Si	Fe	Cu	Cr	Zn	Ti	Mn
Percentage	96.20	1.00	0.80	0.70	0.40	0.35	0.25	0.15	0.15

Table 2: Properties of AA6061 alloy and Si_3N_4.

Properties	Density g/cc	Young's modulus GPa	Tensile strength MPa	Melting temperature °C	Thermal conductivity W/m.K	Linear thermal expansion coefficient —	Specific heat capacity —
AA6061	2.7	68	124-290	585	151-202	2.32×10^{-5}	897 J/kg.K
Si_3N_4	3.21	310	—	1600 (inert)	21	4.3	0.7 J/g°C

(a)

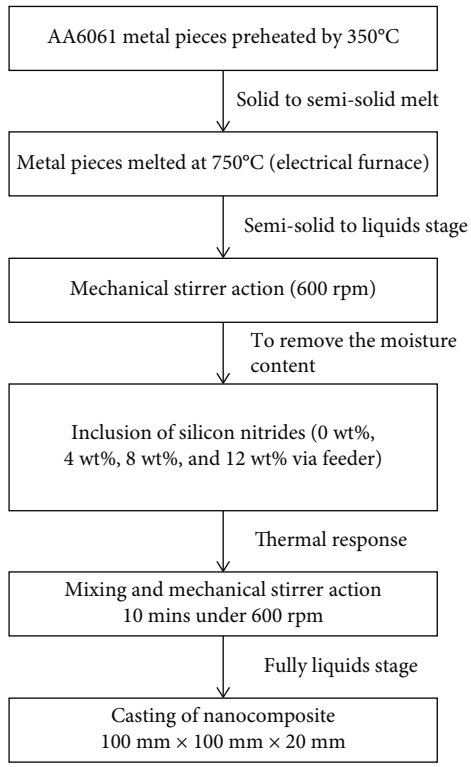

(b)

Figure 1: Aluminium-melting furnace (a) actual fabrication setup and (b) flow process chart for AA6061 alloy nanocomposites.

Table 3: Weight percentages of matrix and reinforcements.

Sample	Constitutions of composites in weight percentages (wt%) AA6061	Si_3N_4
A	100	0
B	96	4
C	92	8
D	88	12

principle of Archimedes as referred from Equation (1). Its values are represented in Figure 3 bar chart-coloured red. It has been observed from Figure 3 bar chart that the level of porosity was decreased with increased content of reinforcement. It was due to continuous stir action during the semisolid stage with a maintained temperature of 300°C to 528°C. Similarly, Fayomi et al. [12] reported that the constant stir speed developed by aluminium alloy composite has less porosity and enhanced mechanical properties. The nanocomposite contained 12 wt% of silicon nitrides and was found at the minor porosity level of 0.88%. It was identified that the porosity of the composite decreased by 23.47% compared to cast AA6061 alloy.

$$\text{Level of porosity in\%} = (1) - \left\{\frac{\text{Actual density}}{\text{Theoretical density}}\right\} \times 100. \quad (1)$$

2.5. Effect of Si_3N_4 and Constant Stir Action on the Microstructure of AA6061 Alloy Nanocomposites.

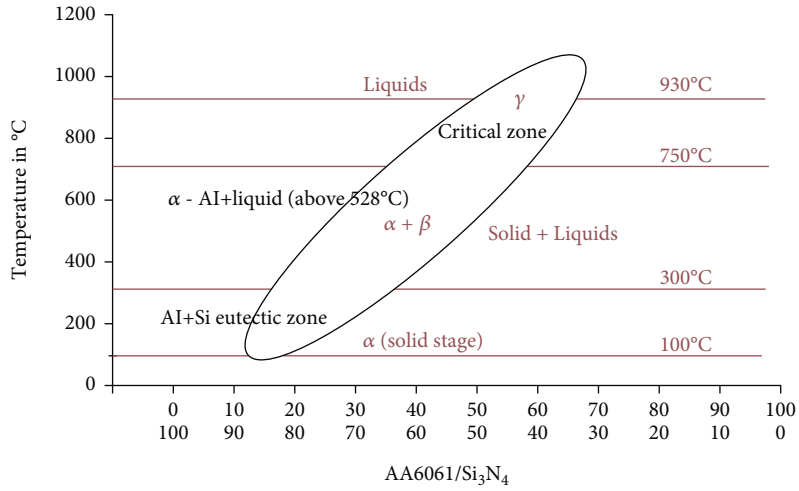

Figure 2: Phase transformation diagram for AA6061/Si_3N_4 nanocomposites with their various phase zone.

Table 4: Experimental test results for AA6061 alloy nanocomposite.

Sample	Density in g/cc		Porosity	Weight loss at 700°C	Heat flow at 700°C	Micro Vickers hardness	Wear rate (80 N)
	Theoretical	Actual	In %	In mg	In mW	In Hv	In $\times 10^{-5}$ m^3/nm
A	2.701	2.67	1.15	45.12	4	29	13.5
B	2.813	2.784	1.03	123.76	5	38	12.8
C	2.832	2.804	0.99	115.29	7	42	11.6
D	2.857	2.832	0.88	84.62	9	46	10.7

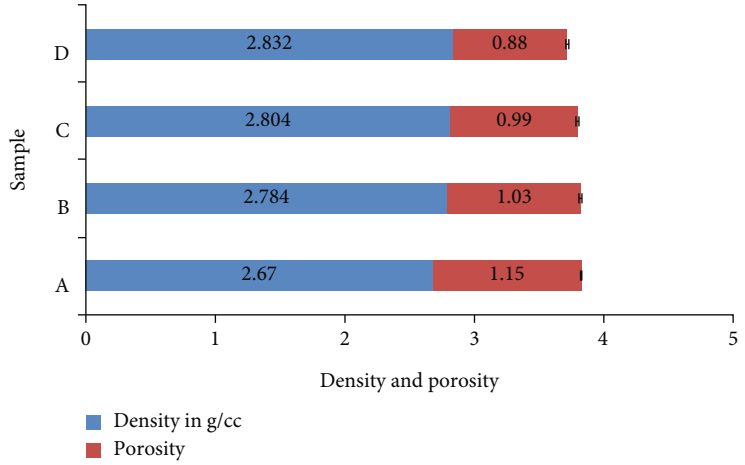

Figure 3: Density and porosity of AA6061/Si_3N_4 nanocomposite.

Figures 4(a)–4(d) illustrate the scanning electron microscope image of AA6061 alloy and 4 wt%, 8 wt%, and 12 wt% Si_3N_4-reinforced AA6061 alloy nanocomposites. Figure 4(a) shows a clear view of the microstructure with microspores. It was evidenced by the experimental test results mentioned in Table 4 and its level was represented in Figure 3. The composite contained 4 wt% and 8 wt% of Si_3N_4, showing uniform nanoparticle distribution in the AA6061 matrix as indicated by a white dot. The enlarged view of Si_3N_4 nanoparticle presence in the AA6061 alloy matrix is shown in Figure 4(d). It shows good interfacial bonding between AA6061 alloy and Si_3N_4, resulting in increased mechanical, thermal, and wear resistance properties. It was due to the applied continuous stir speed of 600 rpm. A similar trend was reported by Fayomi et al. [12] and Chandradass et al. [17] during the evaluation of aluminium alloy (AA8011 and AA6061) composites.

2.6. Effect of Si_3N_4 on the Thermal Response of AA6061 Nanocomposite. The effect of silicon nitrides on the thermal behaviour of AA6061 alloy and 4 wt%, 8 wt%, and 12 wt% Si_3N_4-reinforced AA6061 alloy nanocomposite was proficient by using differential thermal and thermogravimetric analysis apparatus. It was evaluated by the temperature range of 0°C to 700°C, as shown in Figures 5(a)–5(d). It

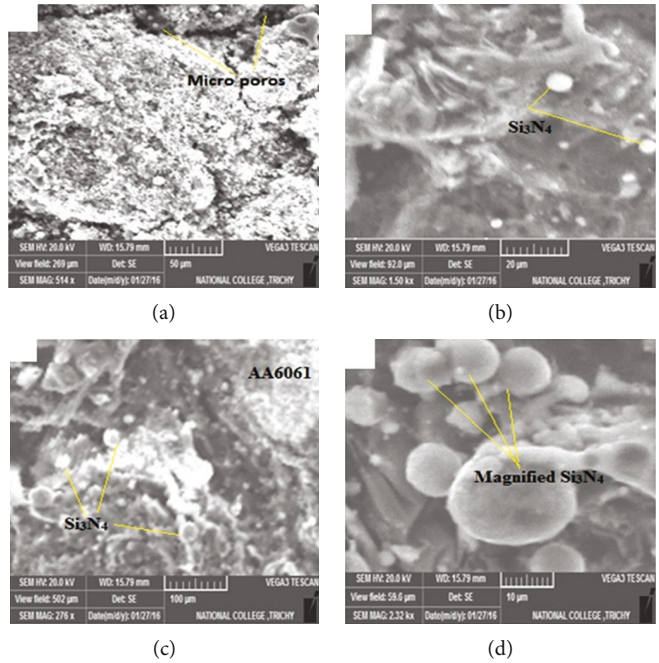

FIGURE 4: SEM image of AA6061 alloy nanocomposites (a) AA6061 alloy, (b) AA6061/4 wt% Si_3N_4, (c) AA6061/8 wt% Si_3N_4, and (d) AA6061/12 wt% Si_3N_4 nanocomposites.

was observed from Figures 5(a)–5(d) that the weight loss of both cast AA6061 alloy and its Si_3N_4-reinforced nanocomposites during the evaluation of a specific temperature range under a steady state heat flow rate of 27°C/min showed a downtrend. It was due to the effect of solubility on the AA6061 matrix at higher temperatures (more than 528°C). The different solubility phase transformation conditions are evidenced in Figure 2.

It was revealed in Figure 5(a) that the thermogravimetric analysis of unreinforced AA6061 alloy shows 45.12 ± 0.03 mg and was reduced to 6.2% compared to ambient temperature mass loss. It was varied due to the different phase temperatures, as evidenced in Figure 2. The incorporation of silicon nitrides into the AA6061 alloy matrix shows higher thermal stability (700°C) with reduced mass loss of 84.62 ± 0.51 mg. It is evidenced from Figures 5(b)–5(d) that the mass loss rate is directly proportional to the temperature, so the thermal performance of the nanocomposite is stable and the material savings is more than 15%. It helps to increase molten metal's fluidity during the composite's casting.

The thermogravimetric analysis helps to increase the material's thermal stability at high temperatures and plays a vital role during solid-to-liquid transition monitoring. Figure 4(d) illustrates that the AA6061 alloy nanocomposite, which contained 12 wt% of Si3N4, increases the temperature of the liquid and acts as a gathering of discontinuous secondary phase has a reduced weight fraction of 84.62 ± 0.51 mg at 700°C. Similarly, Fayomi et al. [18] studied the thermal, electrical, and corrosion characteristics of AA8011/Si_3N_4 alloy composite and reported that silicon nitrides' presence enhances thermal stability at higher temperature and increase thermal conductivity.

2.7. Effect of Si_3N_4 on Heat Flow of AA6061/Si_3N_4 Nanocomposite. Differential thermal analysis for heat flow of aluminium alloy (AA6061) and its Si_3N_4 reinforced AA6061 nanocomposite is shown in Figure 6. The heat flow of AA6061 alloy nanocomposite gradually increases with an increase in the content of silicon nitrides then it was falling at an increased temperature range of 460°C. It is the evidence of heat flow thermometric features at 460°C, 470°C, 476°C, and 480°C on the intermetallic effect of AA6061 alloy during the solid-to-liquid phase transformation as proved in Figure 2 on different weight percentages of silicon nitrides. Arribas and Martín [19] studied and reported that the intermetallic compounds of the composites were located at ϕ-$CuAl_2$ and $Cu_2Mg_8Si_6Al_5$ under 535°C. It shows an Al liquid-phase and Si_3N_4 solid-phase bonded uniformly at 550°C. It is evidenced in Figure 4(d). One researcher used thermal-captured images for routine life prediction [20, 21]. The maximum heat flow of 9 mW was 12 wt% Si_3N_4-reinforced AA6061 nanocomposite. It was increased by 55% and located at 460°C compared to cast AA6061 alloy.

2.8. Effect of Si_3N_4 on the Hardness of AA6061/Si_3N_4 Nanocomposite. Figure 7 illustrates the histogram representation of Vickers (micro) hardness number (VHN) of AA6061/Si_3N_4 alloy nanocomposite. It is noted from Figure 7 that the VHN of AA6061 alloy is 29 ± 1.2 Hv, the additions of 4 wt%, 8 wt%, and 12 wt% of Si_3N_4 shows a 38 ± 1.13 Hv, 42 ± 0.78 Hv, and 46 ± 1.1 Hv, respectively. The maximum 46 ± 1.1 Hv is observed in 12 wt% Si3N4-reinforced AA6061 alloy nanocomposite due to the uniform distribution of reinforcement in the AA6061 matrix, as proved in Figure 4(d). It has increased by 40% as compared

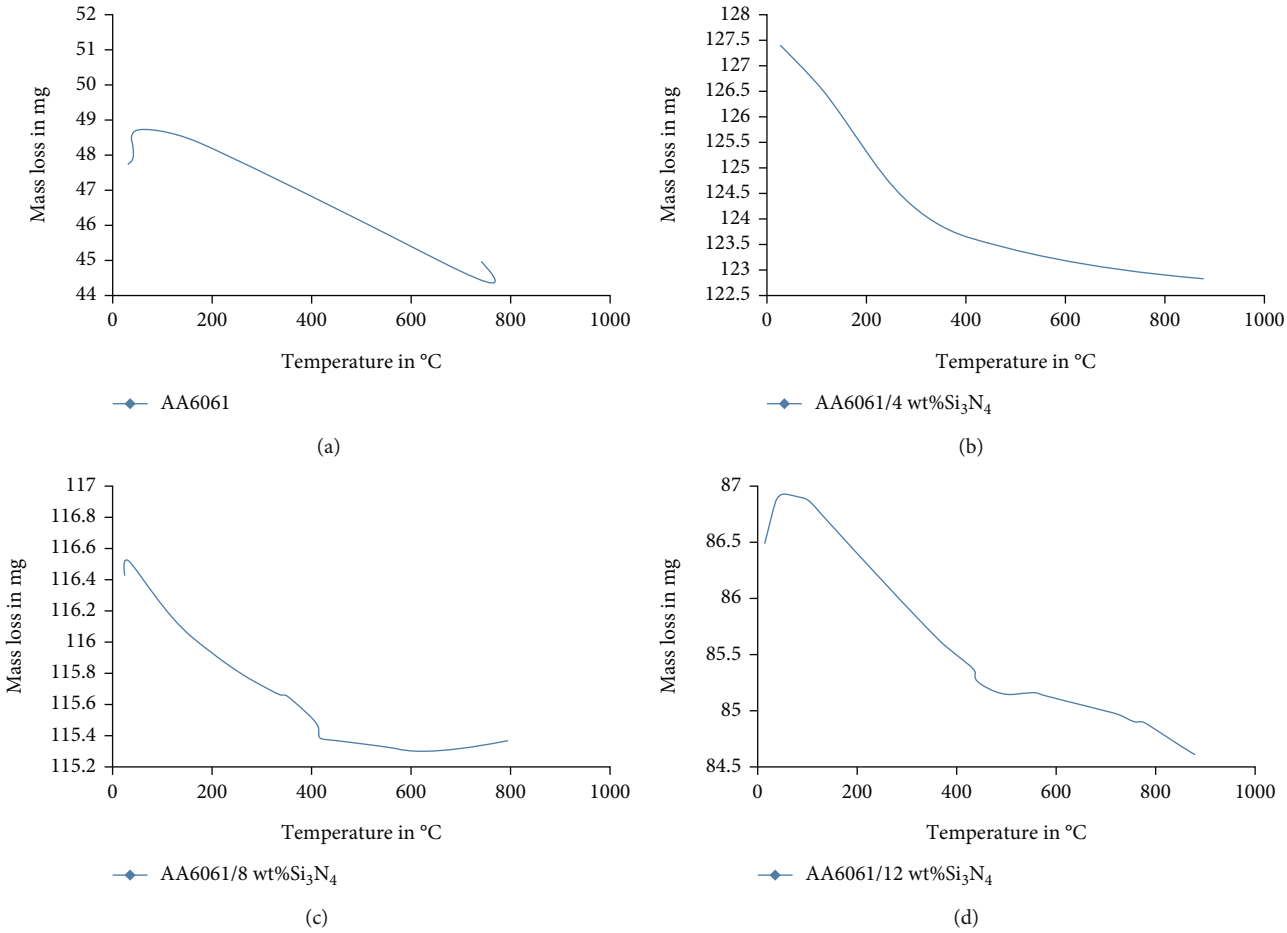

Figure 5: (a) Thermogravimetric analysis for AA6061/0 wt% Si_3N_4. (b) Thermogravimetric analysis for AA6061/4wt% Si_3N_4. (c) Thermogravimetric analysis for AA6061/8wt% Si_3N_4. (d) Thermogravimetric analysis for AA6061/12wt% Si_3N_4.

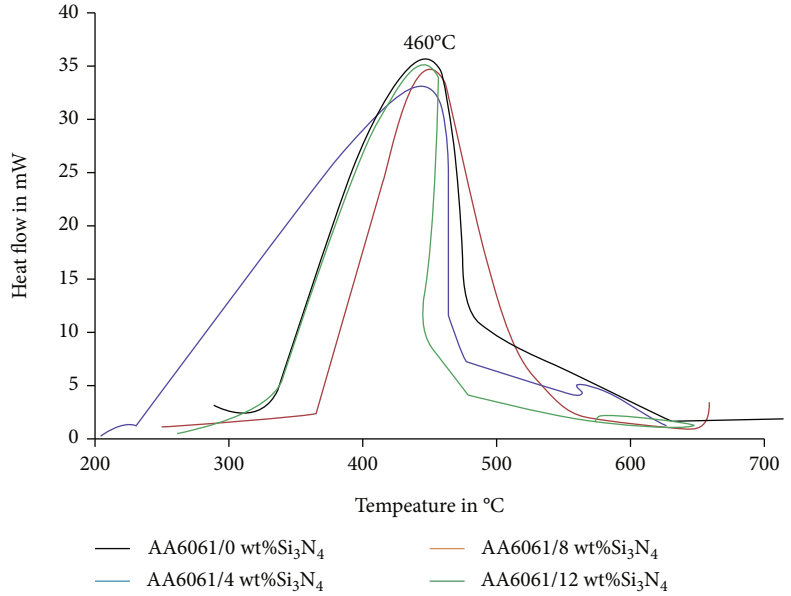

Figure 6: Heat flow analysis of AA6061/Si_3N_4 alloy nanocomposite.

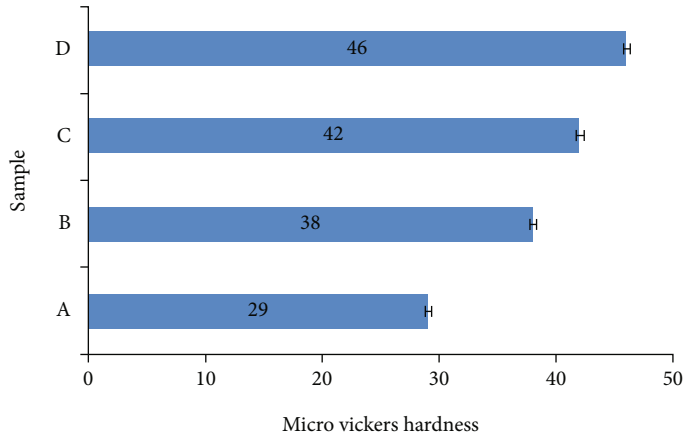

Figure 7: Micro Vickers hardness number of AA6061/Si_3N_4 alloy nanocomposite.

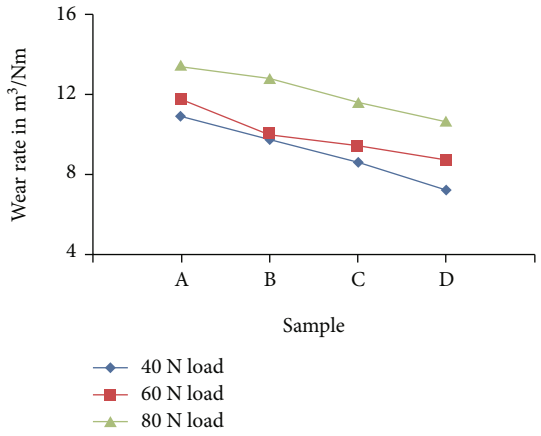

Figure 8: Dry-state wear rate of AA6061/Si_3N_4 alloy nanocomposite (sample A- AA6061/0 wt% Si_3N_4, B- AA6061/ 4 wt% Si_3N_4, AA6061/8 wt% Si_3N_4, and D- AA6061/12 wt% Si_3N_4).

to cast AA6061 alloy. The stirring speed of 600 rpm leads to an increase the particle distribution as well as an increased wettability. So the presence of Si3N4 in AA6061 alloy resisted the internal reimbursement during the dimple against the indenter and the dislocations of particles were limited by good bonding strength between the matrix and reinforcements.

2.9. Effect of Si_3N_4 on Wear Characteristics of AA6061/Si_3N_4 Nanocomposite. The dry-state wear performance of AA6061 alloy and AA6061/Si_3N_4 nanocomposites was tested by a pin-on-disc wear test machine attached with carbon steel disc (168 Hv) operated under the sliding velocity of 1.25 m/ sec at an applied load 40 N, 60 N, and 80 N, respectively. It is seen from Figure 8 that the wear rate of the composite gradually increased with increasing the applied load under constant sliding velocity. However, increased content (4, 8, and 12 wt%) of Si_3N_4 in the AA6061 alloy matrix has reduced wear rates on 40, 60, and 80 N loads. The physical presence of nitride-based reinforcements withstands the high-friction load [15]. The least wear rate of 7.23×10^{-5} m^3/Nm is found on 12 wt% Si_3N_4-reinforced AA6061 nanocomposite under an applied load of 40 N at 1.25 m/sec sliding speed. However, the wear rate of nanocomposite is progressively increasing with the load from 40 N to 80 N.

3. Conclusions

The aluminium alloy nanocomposite contains different weight percentages of 0 wt%, 4 wt%, 8 wt%, and 12 wt% of silicon nitrides effectively developed by liquid state stir cat process with an applied stir speed of 600 rpm on the higher melting temperature of 750°C. The following experimental test results are concluded below.

(1) Rule of the mixture and Archimedes Principle studied the density and porosity of AA6061/ Si_3N_4 alloy nanocomposite, and the nanocomposite containing 12 wt% silicon nitrides found a low porosity level of 0.88% as compared to all other compositions

(2) The phase transformation of AA6061 alloy and the thermal adsorption effect of Si_3N_4 was plotted and explained. The various phases are illustrated in Figure 2

(3) AA6061/12 wt% Si_3N_4 alloy nanocomposite was found to have good thermal stability and minimum weight loss of 84.62 ± 0.51 mg at 700°C

(4) The sufficient heat adsorption of AA6061/12 wt% Si_3N_4 alloy nanocomposite was obtained as 9 mw at 480°C temperature. Its efficiency increased by 55% compared to unreinforced AA6061 alloy

(5) The hardness and wear resistance of AA6061/12 wt% Si_3N_4 alloy nanocomposite were enhanced to 37% and 20% compared to AA6061 alloy

(6) So, the composite containing 12 wt% of Si_3N_4 alloy nanocomposite is applied for the automobile—floor and rooftop applications

Data Availability

All the data required are available within the manuscript.

Conflicts of Interest

Authors declare no conflicts of interest.

References

[1] K. P. Rohatgi, P. Ajaykumar, N. M. Chelliahand, and T. P. D. Rajan, "Solidification processing of cast metal matrix composites over the last 50 years and opportunities for the future, the minerals, metals & materials society," *JOM*, vol. 72, no. 8, pp. 2912–2926, 2020.

[2] A. K. Sharma, A. Aherwar, and R. Rimasauskiene, "Matrix materials used in composites: A comprehensive study," *Materials Today: Proceedings*, vol. 21, pp. 1559–1562, 2020.

[3] E. A. M. Shalaby, A. Y. Churyumov, D. H. A. Besisa, A. Daoud, and M. T. Abou El-Khai, "A comparative study of thermal conductivity and tribological behavior of squeeze cast A359/AlN and A359/SiC composites," *Journal of Material Engineering and Performance*, vol. 26, no. 7, pp. 3079–3089, 2017.

[4] K. U. Kainer, "Metal matrix composites: custom-made materials for automotive and aerospace engineering," Wiley-VCH Verlag GmbH & Co. KGaA, Weinheim, 2006.

[5] D. J. Lloyd, "Particle reinforced aluminium and magnesium matrix composites," *International Materials Reviews*, vol. 39, no. 1, pp. 1–23, 1994.

[6] A. M. Cardinale, D. Macci, G. Luciano, E. Canepa, and P. Traverso, "Thermal and corrosion behaviour of as-cast Al-Si alloys with rare earth elements," *Journal of Alloy's Compounds*, vol. 695, pp. 2180–2189, 2017.

[7] S. Yashpal, C. S. Jawalkar, A. S. Verma, and N. M. Suri, "Fabrication of aluminium metal matrix composites with particulate reinforcement: a review," *Material Today Proceedings*, vol. 4, no. 2, pp. 2927–2936, 2017.

[8] N. Panwar and A. Chauhan, "Fabrication methods of particulate reinforced aluminium metal matrix composite-a review," *Material Today Proceedings*, vol. 5, no. 2, pp. 5933–5939, 2018.

[9] C. S. Ramesh, R. Keshavamurthy, and J. Madhusudhan, "Fatigue behavior of Ni-P coated Si_3N_4 reinforced Al6061 composites," *Procedia Materials Science*, vol. 6, pp. 1444–1454, 2014.

[10] C. S. Ramesh, R. Keshavamurthy, B. H. Channabasappa, and A. Ahmed, "Microstructure and mechanical properties of Ni-P coated Si_3N_4 reinforced Al6061 composites," *Material Science and Engineering Part A*, vol. 502, no. 1-2, pp. 99–106, 2009.

[11] X. Bai, C. Huang, J. Wang, B. Zou, and H. Liu, "Fabrication and characterization of Si_3N_4 reinforced Al_2O_3-based ceramic tool materials," *Ceramics International*, vol. 41, no. 10, pp. 12798–12804, 2015.

[12] J. Fayomi, A. P. I. Popoola, O. P. Oladijo, O. M. Popoola, and O. S. I. Fayomi, "Experimental study of ZrB_2-Si_3N_4 on the microstructure, mechanical and electrical properties of high grade AA8011 metal matrix composites," *Journal of Alloys and Compounds*, vol. 790, pp. 610–615, 2019.

[13] X. Zhu, Y. Zhou, and K. Hirao, "Effect of sintering additive composition on the processing and thermal conductivity of sintered reaction-bonded Si_3N_4," *Journal of American Ceramic Society*, vol. 87, no. 7, pp. 1398–1400, 2004.

[14] R. Karthik, K. Gopalakrishnan, R. Venkatesh, A. Mohana Krishnan, and S. Marimuthu, "Influence of stir casting parameters in mechanical strength analysis of aluminium metal matrix composites (AMMCs)," *Materials Today Proceedings*, vol. 62, no. 4, pp. 1965–1968, 2022.

[15] I. S. Han, D. W. Seo, S. Y. Kim, K. S. Hong, K. H. Guahk, and K. S. Lee, "Properties of silicon nitride for aluminum melts prepared by nitrided pressureless sintering," *Journal of the European Ceramic Society*, vol. 28, no. 5, pp. 1057–1063, 2008.

[16] M. O. Mazahery and M. O. Shabani, "Extruded AA6061 alloy matrix composites: the performance of multi-strategies to extend the searching area of the optimization algorithm," *Journal of Composite Materials*, vol. 48, no. 16, pp. 1927–1937, 2014.

[17] J. Chandradass, T. Thirugnanasambandham, P. Jawahar, and T. T. M. Kannan, "Effect of silicon carbide and silicon carbide/alumina reinforced aluminum alloy (AA6061) metal matrix composite," *Materials Today: Proceedings*, vol. 45, pp. 7147–7150, 2021.

[18] J. Fayomi, A. P. I. Popoola, O. M. Popoola, and O. S. I. Fayomi, "The appraisal of the thermal properties, electrical response, and corrosion resistance performance of AA8011 reinforced Nano Si_3N_4 for automobile application," *Journal of Alloys and Compounds*, vol. 850, article 156679, 2021.

[19] J. M. Arribas, F. C. Martín, and F. Castro, "The initial stage of liquid phase sintering for an Al-14Si-2.5Cu-0.5Mg (wt%) P/M alloy," *Material Science Engineering A*, vol. 527, no. 16-17, pp. 3949–3966, 2010.

[20] C. Ramesh Kannan, S. Manivannan, and M. Vivekanandan, "Synthesis and experimental investigations of tribological and corrosion performance of AZ61 magnesium alloy hybrid composites," *Journal of Nanomaterials*, vol. 2022, Article ID 6012518, 12 pages, 2022.

[21] A. Mohana Krishnan and M. Dineshkumar, "Evaluation of mechanical strength of the stir casted aluminium metal matrix composites (AMMCs) using Taguchi method," *Materials Today Proceedings*, vol. 62, no. 4, pp. 1943–1946, 2022.